SPACE WEATHERING MAPS OF THE LUNAR POLES USING KAGUYA SPECTRAL PROFILER DATA. D. Trang[1], M. Lemelin[2], S. T. Crites[3], and P. G. Lucey[1], [1]Hawai'i Institute of Geophysics and Planetology, University of Hawai'i at Mānoa, Honolulu, HI (dtrang@higp.hawaii.edu), [2]York University, Toronto, ON, Canada, [3]Japan Aerospace Exploration Agency, Institute of Space and Astronautical Science (JAXA/ISAS), Japan.

Introduction: Lunar space weathering encompasses a number of space-surface interactions, including micrometeoroid, solar wind, and cosmic rays bombardment [1–4]. The degree these processes affects the surface is dependent on its latitude. Several workers have suggested that the degree of space weathering is weaker towards the poles than the equatorial regions. Yokota et al. (2011) found that high latitude highlands display higher reflectances and bluer slopes than highlands in equatorial areas suggesting less intense space weathering in areas closer to the poles [5]. Hemingway et al. (2015) noticed that mare regions along the equator are darker with higher 950/750 nm reflectance ratios (i.e., redder) than mare at high latitudes [6]. They indicate it is due to reduced solar wind flux towards the poles, which is also supported by Lemelin et al. (2016) [7]. Sim et al. (2017) found that craters in higher latitudes had greater OMAT values than craters in lower latitudes, supporting a latitudinal dependency of space weathering [8].

An important product of the space weathering process on the Moon is the formation of submicroscopic iron particles because their presence strongly affects the visible to near infrared spectral properties of lunar material [9]. The optical effects of submicroscopic particles are bimodal with size. Particles much smaller than the wavelength of light (nanophase iron) both darken and redden visible and near-infrared spectra of transparent host material. Particles somewhat larger than the wavelength of light (microphase iron) darken, but do not redden it [10,11]. By using these contrasting spectral characteristics of nanophase and microphase iron particles, Trang et al. (2017) and Trang and Lucey (2019) produced nanophase and microphase particle abundance maps of both Mercury and the Moon [12,13]. However, their maps are more reliable in the equatorial regions than the poles because the lighting geometry at the poles are less than ideal (low Sun angles). In this study, we will use radiometrically calibrated Kaguya Spectral Profiler (SP) data of the poles and the Hapke radiative transfer model [9,11] to investigate the nanophase and microphase iron abundances across the lunar poles.

Methods: We use the radiometrically calibrated Kaguya Spectral Profiler (SP) radiance data converted to diffuse reflectance (level 2B1) at 750, 950 and 1550 nm to model the abundance of submicroscopic particles with the Hapke radiative transfer model. The reflectance in these three bands allows us to capture the slope of the continuum. We used SP data that was acquired during the north and south polar summers (orbits ~2000-2999 and orbits ~4000-4999) to maximize the extent of illuminated areas and the strength of the signal [5]. We apply the photometric function of Yokota et al. [2011] to correct for the observational geometry in the SP data [5]. This photometric function assumes a flat surface, thus there are important residual errors on topographic slopes. Therefore, the abundances of submicroscopic particles modeled herein are reliable on flat surfaces only.

To model the SP data, we make several assumptions about the regolith. First the regolith consists mostly of silicates. Trang and Lucey (2019) created a spectral model that can determine the reflectance of lunar silicates based upon its FeO content [13]. For the lunar poles, we are able to determine the appropriate model reflectance by using a FeO map developed by Lemelin et al. (2017) [15]. We also assume that the regolith contains about 1 wt% ilmenite, which is consistent with the model abundance throughout the lunar highlands from Sato et al. (2017) [14]. Although the model of Sato et al. (2017) is not appropriate for small abundances of titanium, the samples analyzed by the Lunar Soil Characterization Consortium contained ilmenite abundances greater than 0 wt%. In our model, we input the single scattering albedo of ilmenite. Next, we add the nanophase and microphase iron at various abundances (i.e., from 0–1.5 wt% at intervals of 0.01 wt%) into the host particles via the radiative transfer technique resulting in thousands of model spectra, which builds our spectral library. Next, we compared the reflectance at 750, 950, and 1550 nm of each SP "spectrum" (pixel) to each model spectrum in the spectral library. The model spectrum with the lowest RMS is the best fitting spectrum its corresponding nanophase and microphase iron abundances are assigned to that given pixel.

After acquiring the nanophase and microphase iron abundance from each SP spectrum, we map the results using the Generic Mapping Tool (GMT). We also apply a surface filter, which uses adjustable tension continuous curvature splines to interpolate between data points.

Results and Discussion: We found that we are able to closely model the majority of the SP data, but with better consistency with the north pole more than

the south pole. We mapped the abundances onto six polar projected maps. Of the six maps, three are of the north pole and three are of the south pole. Of those three maps of each pole, they consist of a nanophase (**Fig. 1** and **2)**, microphase (**Fig. 1** and **2)**, and a combined nanophase and microphase iron abundance (i.e., submicroscopic iron abundance) maps for each pole.

In **Fig. 1** and **2**, we observe that the topography influences our resulting abundances, which is best observed on crater walls (**Fig. 1** and **2**). Overall (including pixels covering topographic slopes), we find that towards both poles, the nanophase iron abundances decreases towards the poles, whereas the south pole microphase iron abundance shows a steady decrease, but the north pole microphase iron abundance is nearly constant with a slight decrease after 80° latitude (**Fig. 3**). This may be attributed to the decreased flux in solar wind and micrometeoroid impacts [5–8].

Future Work: Fig. 1 and **2** show topographic dependencies in which we will make topographic corrections to the SP data. In addition, we plan to relook at the spectral fits between the model spectra and the SP data to improve fits. After making these two corrections, we will reexamine the relationship between submicroscopic iron particle abundance and latitude to determine if we see the same pattern (i.e., decreases in abundance poleward).

References: [1] Housley et al. (1973), Proc. Lunar Sci. Conf. 4th, 2737–2749; [2] McKay et al. (1974), Proc. Lunar Sci. Conf. 5th, 887–906; [3] Reed and Arnold (1972), JGR, 77, 537–555; [4] Horz et al. (1971), JGR, 76, 5770–5798; [5] Yokota et al. (2011), Icarus, 215, 639–660; [6] Hemingway et al. (2015), Icarus, 261, 66–79; [7] Lemelin et al. (2016), Icarus, 273, 315–328; [8] Sim et al. (2017), GRL, 44, 11273–11281; [9] Hapke (2001), JGR, 106, 10039–10073; [10] Noble et al. (2007), Icarus, 192, 629–642; [11] Lucey and Riner (2011), Icarus, 212, 451–462; [12] Trang et al. (2017), Icarus 293, 206–217; [13] Trang and Lucey (2019), Icarus, 321, 307–323; [14] Sato et al. (2017), Icarus, 296, 216–238; [15] Lemelin et al. (2017), LPSC 48, abstract 2479.

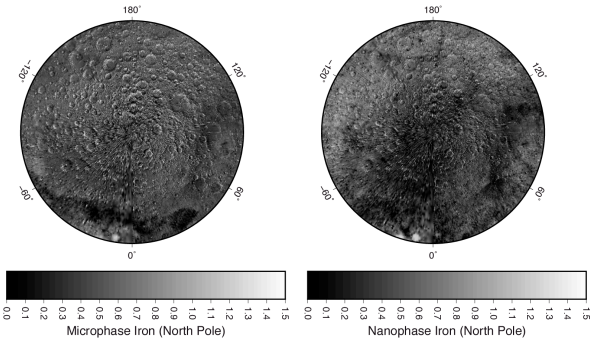

Fig. 1: Nanophase and microphase iron abundance of the north pole.

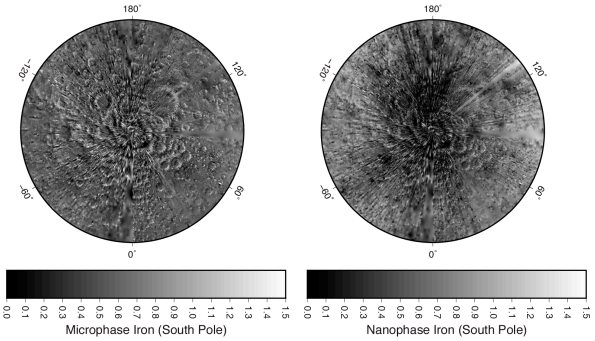

Fig. 2: Nanophase and microphase iron abundance of the south pole.

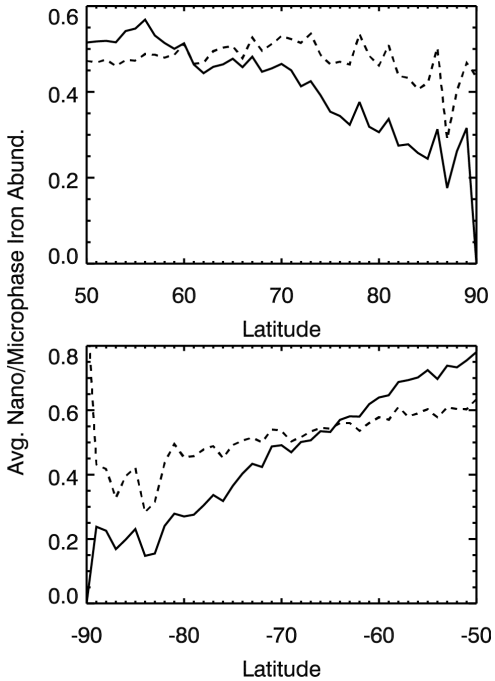

Fig. 3: Average nanophase (solid) and microphase (dashed) iron abundance in the north and south poles.